Delivery of the p38 MAPkinase Inhibitor SB202190 to Angiogenic Endothelial Cells: Development of Novel RGD-Equipped and PEGylated Drug−Albumin Conjugates Using Platinum(II)-Based Drug Linker Technology

Kai Temming,*[,†,‡] Marie Lacombe,[†] Paul van der Hoeven,[†] Jai Prakash,[‡] Teresa Gonzalo,[‡] Eli C. F. Dijkers,[∥] László Orfi,[⊥] Gyorgy Kéri,[#] Klaas Poelstra,[‡] Grietje Molema,[§] and Robbert J. Kok[‡,▽]

KREATECH Biotechnology B.V., Amsterdam, The Netherlands, Department of Pharmacokinetics and Drug Delivery, Groningen University Institute of Drug Exploration, Groningen, The Netherlands, Medical Biology Section, Department of Pathology and Laboratory Medicine, University Medical Center Groningen, University of Groningen, The Netherlands, Department of Nuclear Medicine and Molecular Imaging, University Medical Center Groningen, Groningen, The Netherlands, Department of Pharmaceutical Chemistry, Semmelweis University, Budapest, Hungary, and Department of Medical Chemistry, Peptide Biochemistry Research Group of the Hungarian Academy of Sciences, Semmelweis University, Budapest, Hungary.
Received January 23, 2006; Revised Manuscript Received June 14, 2006

Endothelial cells play an important role in inflammatory disorders, as they control the recruitment of leukocytes into inflamed tissue and the formation of new blood vessels. Activation of p38MAP kinase results in the production of proinflammatory cytokines and the expression of adhesion molecules. P38MAP kinase inhibitors are therefore considered important candidates for the treatment of inflammatory disorders. In the present study, we propose a novel strategy to counteract these processes by delivery of the p38MAP kinase inhibitor SB202190 into angiogenic endothelial cells. A drug-targeting conjugate was developed by conjugation of SB202190 to human serum albumin (HSA) using a novel platinum-based linker. Specificity for angiogenic endothelial cells was introduced by conjugation of cyclic RGD-peptides via bifunctional polyethylene glycol linkers. The final products contained an average of nine SB202190 and six RGDPEG groups per albumin. The platinum-based linker displayed high stability in buffers and culture medium, but released SB202190 slowly upon competition with sulfur-containing ligands like glutathione. RGDPEG−SB−HSA bound to α_{v3}-integrin expressing endothelial cells (human umbilical cord vein endothelial cells) with low nanomolar affinity and was subsequently internalized. When HUVEC were treated with TNF to induce inflammatory events, pretreatment with RGDPEG−SB−HSA partially inhibited proinflammatory gene expression (IL-8, E-selectin; 30% inhibition) and secretion of cytokines (IL-8, 34% inhibition). We conclude that the developed RGDPEG−SB−HSA conjugates provide a novel means to counteract inflammation disorders such as rheumatoid arthritis.

INTRODUCTION

In chronic inflammatory diseases, endothelial cells are a key player in induction and progression of the disease. Proinflammatory proteins like TNFα and IL-1β induce signaling via p38MAP kinase and NFκB to activate endothelial cells (*1*). The activated endothelial cell excrete cytokines and chemokines (IL-8, IL-6), which in concert with cellular adhesion molecules (P-selectin, E-selectin, VCAM, ICAM) promote leukocyte recruitment and infiltration, and mediate vascular remodeling (*2*, *3*). Signal transduction inhibitors have been developed to interfere with these processes (*4*−*6*), and especially, inhibitors of the p38MAP kinase are considered promising candidates for treatment of chronic inflammation (*7*, *8*). Despite promising results in preclinical inflammation models, most of the p38MAP kinase inhibitors have failed in phase II clinical studies due to unacceptable side effects. Local delivery of the inhibitor to endothelial cells may overcome this problem. Previously, we developed RGD-equipped conjugates that bind to $\alpha_v\beta_3$-integrin and are internalized by endothelial cells (*9*−*11*).

In the present paper, we investigate how activation of endothelial cells can be inhibited by a drug delivery approach, in which the p38MAP kinase inhibitor SB202190 is delivered to angiogenic endothelium. For the purpose of intracellular delivery of SB202190, we designed a macromolecular conjugate of drug, carrier backbone, and homing device (Figure 1). In the past, we succesfully applied the carrier protein human serum albumin (HSA) for drug delivery to the liver (*12*). HSA functions as a natural polymer featuring long circulation times, high biocompatibility, and excellent biodegradability that can be readily modified with drugs and targeting ligands. A novel type of platinum-based linker chemistry was applied to conjugate SB202190 to HSA. This linker, which has been named universal linkage system (ULS), binds SB202190 via a coordination linkage at the pyridyl nitrogen of SB202190 (Figure 2), and another coordination bond is formed with methionine or histidine

* Corresponding author. Kai Temming, Department of Pharmacokinetics and Drug Delivery, Groningen University Institute of Drug Exploration, Antonius Deusinglaan 1, 9813 AV, Groningen, The Netherlands. Email: k.temming@rug.nl. Tel: +31 50 363 7627. Fax: +31 50 363 3247.

[†] KREATECH Biotechnology B.V.

[‡] Department of Pharmacokinetics and Drug Delivery, Groningen University Institute of Drug Exploration.

[§] Department of Pathology and Laboratory Medicine, University Medical Center Groningen.

[∥] Department of Nuclear Medicine and Molecular Imaging, University Medical Center Groningen.

[⊥] Department of Pharmaceutical Chemistry, Semmelweis University.

[#] Peptide Biochemistry Research Group of the Hungarian Academy of Sciences, Semmelweis University.

[▽] Present affiliation: Department of Pharmaceutics, Utrecht University, The Netherlands.

10.1021/bc0600158 CCC: $33.50
Published on Web 08/10/2006

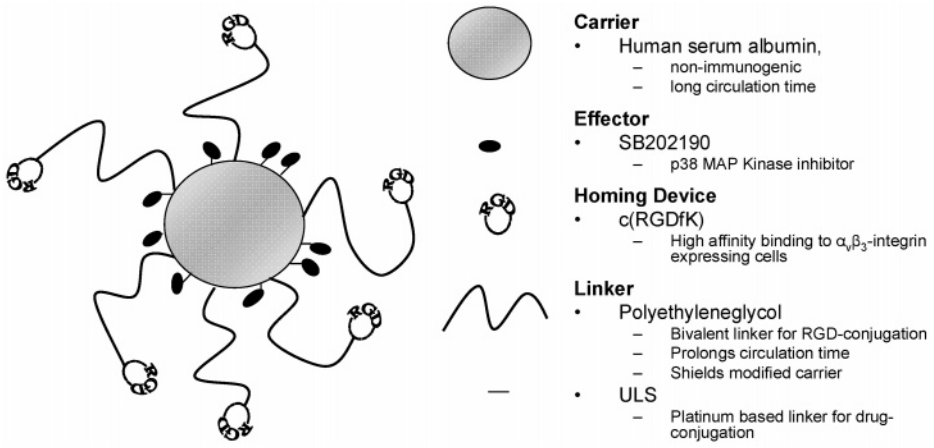

Figure 1. Schematic presentation of drug-targeting construct.

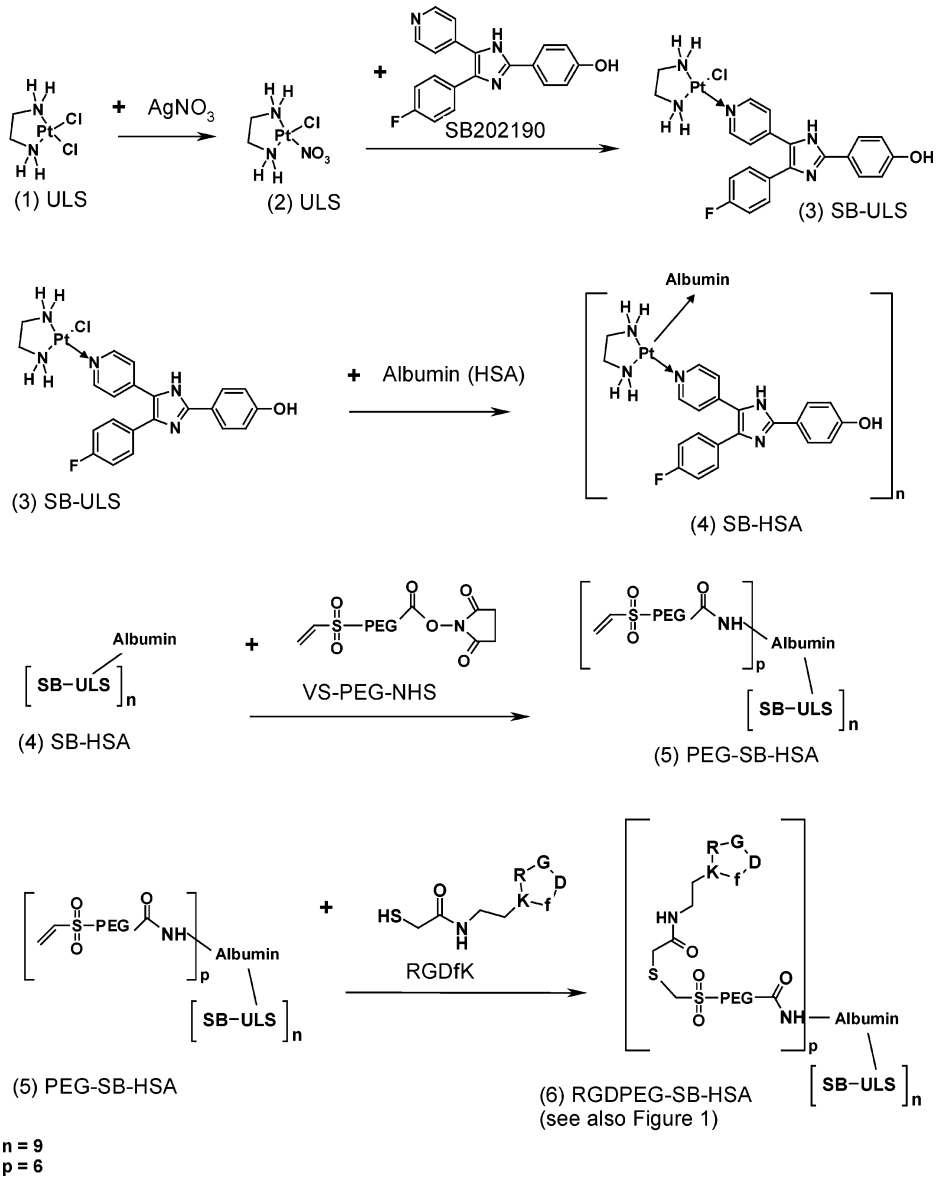

Figure 2. Reaction scheme for synthesis of RGDPEG−SB−HSA.

residues of the carrier (*13*). The stability and release properties of SB−ULS−HSA are reported in this study.

To infer specificity for angiogenic endothelial cells, we attached RGD-peptide targeting ligands to SB−HSA via bivalent 3.5 kDa PEG linkers. These PEG linkers will shield the modifications in the albumin, and thereby will prevent nonspecific uptake, prolong circulation times, and even might lead to passive retention in the leaky vasculature in inflamed tissue (*14*). The appended targeting ligand, cyclic RGDfK pentapeptide, is known to bind with high affinity and specificity to $\alpha_v\beta_3$-integrin, which is expressed in high amounts on angiogenic endothelium (*15*, *16*). Excessive angiogenesis is part of the pathology of

chronic inflammatory disease like rheumatoid arthritis or Crohn's disease. Expression of $\alpha_v\beta_3$-integrin is minimal on resting endothelial cells and highly limited in other healthy tissue. Significant amounts of $\alpha_v\beta_3$-integrin have only been found in osteoclasts (*17*). The restricted expression profile of endothelial cells makes it an ideal target for drug delivery purposes. Moreover, the endothelium is in direct contact with the systemic circulation, which renders these target cells easily accessible for macromolecules and particulate delivery systems. Vascular targeting strategies are therefore an exciting option for therapeutic intervention in chronic inflammation (*18*).

We now report on the synthesis and characterization of the RGDPEG−SB−HSA conjugate. The targeting potential of the product was evaluated on human umbilical cord vein endothelial cells (HUVEC), and pharmacological effects of the delivered drug were studied by its effects on the expression of TNFα-induced gene expression and cytokine secretion.

MATERIALS AND METHODS

Synthesis and Purification of RGDPEG−SB−HSA Conjugate. *Synthesis of SB−ULS. Cis*-[Pt(ethylenediamine)nitrate-chloride] (referred to as ULS, KREATECH Biotechnology, Amsterdam, The Netherlands) was synthesized by reacting *cis*-[Pt(ethylenediamine)dichloride] in *N*,*N*′-dimethylformamide (5 mg/mL) with 1 molar equiv of $AgNO_3$ (51 mM in *N*,*N*′-dimethylformamide (DMF)). Precipitated silver chloride was removed by centrifugation. SB202190 ((4-(fluorophenyl)-2-(4-hydroxyphenyl)-5-(4-pyridyl)-1*H*-imidazole, obtained from L.C. Laboratories, Woburn, MA) was dissolved in DMF at a concentration of 10 mg/mL. Then, 440 μL of the ULS solution (5.18 μmol) was added to 180 μL of the SB202190 solution (5.43 μmol). The resulting solution was heated at 37 °C for 3 h, and the reaction was followed by analytical HPLC using a Luna2 C18 column that was maintained at 40 °C. The mobile phase consisted of a binary solvent system of triethylammonium acetate (100 mM pH 5.0)/acetonitrile 90:10 (solvent A) and triethylammonium acetate (100 mM pH 5.0)/acetonitrile 70:30 (solvent B). The column was eluted at a flow rate of 1.1 mL/min. Compounds were eluted at a stepwise gradient (0% B from 0−4 min; 0−46% B from 4−17 min; 46−100% B from 17−19 min; 100% B from 19−25 min; 100−0% B from 25−27 min; 0% B from 27−34 min). SB202190 eluted at 14.7 min (33.6% B) and SB−ULS eluted earlier (21.8% B). After the reaction was completed, the mixture was evaporated to dryness under reduced pressure, affording a pale yellow solid (yield 92%). SB202190−ULS was analyzed by HPLC ^{1}H NMR and electronspray mass spectrometry.

^{1}H NMR of free SB202190 (CD_3OD): δ_H 6.88 (d, $J = 8.74$ Hz, 2H, $F(CHCH)_2$), 7.17 (m, 2H, $N(CHCH)_2$), 7.50 (m, 4H, $(CHCH)_2OH$), 7.82 (d, $J = 8.68$ Hz, 2H, $F(CHCH)_2$), 8.41 (m, 2H, $N(CHCH)_2$) ppm.

^{1}H NMR of SB202190−ULS (CD_3OD): δ_H 2.59 (m, 4H, $H_2N(CH_2)_2NH_2$), 5.58 (s, 2H, NH_2), 5.91 (s, 2H, NH_2), 6.89 (d, $J = 8.75$ Hz, 2H, $F(CHCH)_2$), 7.22 (m, 2H, $N(CHCH)_2$), 7.53 (m, 4H, $(CHCH)_2OH$), 7.82 (d, $J = 8.73$ Hz, 2H, $F(CHCH)_2$), 8.52 (m, 2H, $N(CHCH)_2$) ppm.

Mass spectrometry of SB202190−ULS (ESI^+): Theoretical mass *m*/*z* of SB−ULS: 620.97 [M]. Detected masses *m*/*z*: 622 $[M + H]^+$, 585 $[M - Cl^- - H^+]^+$.

Starting material of ULS was consumed completely, and formation of a new compound was observed by HPLC analysis. This new peak was SB−ULS as confirmed by LC-MS. SB−ULS was used without further purification in the next reaction step.

Synthesis of SB−ULS−HSA. HSA (22 mg, 325 nmol) was dissolved in 1 mL of 20 mM tricine−NaOH/$NaNO_3$ buffer pH 8.5. SB202190−ULS (3250 nmol) was added in tenfold molar excess, and the mixture was reacted for 24 h at 37 °C, after which nonreacted SB−ULS was removed by dialysis against PBS at 4° C using Slide-A-Lyzer dialysis cassettes (MWCO 10 000 Da, Pierce). The product was sterilized by filtration via a 0.2 μm filter and stored at −20 °C. Conjugation of SB−ULS to the protein was verified by UV analysis at 364 nm. SB−ULS−HSA displayed a specific absorbance at this wavelength ($\epsilon = 13\,955\ M^{-1}\ cm^{-1}$), not found in HSA. SB−ULS−HSA was furthermore characterized for protein content, drug content, and platinum linker content as described below.

Synthesis of RGDPEG−SB−HSA. In the final reaction step, SB−ULS−HSA was modified with PEG and RGD−peptide. SB−ULS−HSA (147 nmol) dissolved in PBS was incubated with a 50-fold molar excess of vinylsulfone−polyethylene glycol−*N*-hydroxysuccinimide ester (VNS−PEG−NHS; Nektar, Alabama; 3.5 kDa, 20 mg/mL in water, 7.39 μmol), which was added dropwise. The mixture was protected from light with aluminum foil and incubated for 1 h at room temperature while gently shaking on a spiramix. Meanwhile, the RGD-peptide c(RGDf(ϵ-*S*-acetylthioacetyl)K) (Ansynth Service, Roosendaal, The Netherlands) was dissolved at 10 mg/mL in a 1:4 acetonitrile/water mixture. The peptide (8.085 μmol) was added dropwise to the reaction mixture in a 55-fold molar excess, after which hydroxylamine was added to a final concentration of 50 mM. Reactions were carried out overnight at room temperature while protecting from light. Remaining VNS groups were quenched by addition of cysteine (8.085 μmol; equivalent to the amount of RGD-peptide), after which the product was dialyzed against PBS, and finally purified by size exclusion chromatography (SEC) on a Superdex200 column on an Äkta System (GE Healthcare, Uppsala, Sweden) using PBS at 0.5 mL/min as the mobile phase. Eluting peaks were monitored simultaneously at 214, 280, and 364 nm. The final products RGDPEG−SB−HSA and RADPEG−SB−HSA were stored at −20 °C. The control conjugate RADPEG−SB−HSA was prepared according to the same protocol with a c(RADf(ϵ-*S*-acetylthioacetyl)K) peptide.

Characterization of RGDPEG−SB−HSA. Protein content was evaluated using BCA protein assay kit (Pierce). Free drug and conjugated drug content were analyzed by isocratic HPLC using a Waters system (Massachusetts) with a C18 μBondapak column and a UV detector operating at 254 nm. SB202190 was eluted with a mixture of water/acetonitrile/trifluoroacetic acid 20/80/0.1 at 1 mL/min. The absence of free SB202190 and SB−ULS in the drug-targeting preparation was determined by analysis of PBS diluted samples (retention times: SB202190, 8.7 min; SB-ULS, 11 min). The amount of SB202190 conjugated to the carrier was determined after release of the drug by overnight incubation with 0.5 M KSCN in PBS at 80 °C. The cooled samples were injected into the HPLC without further sample pretreatment or stored at −20 °C for later HPLC analysis.

The ULS-linker content was evaluated by inductive coupled plasma atomic emission spectroscopy (ICP-AES) at the specific wavelengths of platinum (214.424 and 265.945 nm) on a VISTA AX CCD Simultaneous ICP-AES (Varian, Palo Alto, CA). Standard solutions were made with cisplatin, and yttrium was used as internal standard (360.074 nm).

Intermediate and final products were subjected to analytical SEC to reveal increases in size, purity, and grade of aggregation.

SDS-PAGE (12% ready gels in a mini-Protean II system; Bio-Rad, Veenendaal, The Netherlands) followed by Western blot detection with an in-house-prepared anti-RGD antiserum was performed to detect the presence of RGD-peptide conjugated to the PEGylated albumins (*9*). Duplicate gels were either stained for protein (Coomassie Brilliant Blue staining) or blotted on a PVDF membrane (Roche, Mannheim, Germany). The

membrane was blocked with bovine serum albumin (BSA) and subsequently incubated with rabbit anti-RGD antiserum. The signal was amplified with a polyclonal goat anti-rabbit IgG conjugated with horseradish peroxidase (GARPO, DAKO). Peroxidase was visualized by incubation with 3-amino-9-ethylcarbazole (AEC, Sigma).

The grade of PEGylation was accurately determined by MALDI-TOF analysis using a Voyager-DE PRO workstation (Applied Biosystems). HSA, SB−HSA, and RGDPEG−SB−HSA were dissolved at a concentration of 1 mg/mL in 50:50:0.1 methanol/water/acetic acid. A 1 μL aliquot was mixed with 1 μL of matrix (20 mg/mL sinapinic acid in 60:40:0.1 water/acetonitrile/trifluoroacetic acid), transferred onto a stainless steel sample holder, and dried before being introduced into the mass spectrometer. Mass spectra were obtained by averaging the signals from 100 laser shots. Spectra were calibrated using BSA as a control. MALDI-TOF analysis of BSA provided, among others, signals of single-charged monomeric BSA and of the single-charged dimer of BSA. Our products displayed masses that were inbetween these two calibration peaks. The number of RGDPEG groups bound per albumin was calculated from the averaged masses of the products.

Stability and Drug Release Properties of the SB−ULS Linkage. Appropriately diluted aliquots of SB−ULS−HSA (40 μM) were incubated for 24 h at 37 °C with different matrices to investigate the stability of the conjugate and its drug-releasing properties. Studied matrices were PBS (pH 7.4), 0.1 M sodium acetate buffer (pH 5.0), PBS or acetate buffer spiked with either 5 mM glutathione (GSH) or with 5 mM dithiothreitol (DTT), and endothelial cell (EC) medium containing 20% FCS. Complete release of SB202190 was effected by overnight incubation with 500 mM KSCN at 80 °C. 35 μL of the resulting solutions and standard solutions were treated with 100 μL of acetonitrile (3:1 v/v), vortexed, and centrifuged for 10 min to precipitate proteins. The clear supernatant was subjected to isocratic HPLC analysis as described above.

Cells. HUVEC were obtained from the UMCG Endothelial Cell Facility (*19*). Primary isolates were cultured in 1% gelatin-coated tissue culture flasks or culture wells (Corning, Costar, The Netherlands) at 37 °C under 5% CO_2/95% air. The culture medium, hereafter referred to as EC medium, consisted of RPMI 1640 (BioWittaker, Verviers, Belgium) supplemented with 20% heat-inactivated fetal calf serum (Integro, Zaandam, The Netherlands), 2 mM L-glutamine (Invitrogen, Breda, The Netherlands), 5 U/mL heparin (Leo Pharmaceutical Products, Weesp, The Netherlands), 100 U/mL penicillin (Yamanouchi Pharma, Leiderdorp, The Netherlands), 100 g/mL streptomycin (Radiumfarma-Fisiopharma, Italy), and 50 μg/mL endothelial cell growth factor supplement extracted from bovine brain. After attaining confluence, cells were detached from the surface by trypsin/EDTA (0.5/0.2 mg/mL in PBS) treatment and split into 1:3 ratio. Cells were used up to passage four.

Binding and Uptake of RGDPEG−SB−HSA to HUVEC. Binding affinity of RGDPEG−SB−HSA for target cells was determined by competitive binding studies with ^{125}I-labeled echistatin as $\alpha_v\beta_3$-integrin specific radioligand (*20*). Echistatin was radiolabeled using the chloramine T method (*21*). On the day of the experiment, ^{125}I-echistatin was purified using a PD-10 column (GE Healthcare). Confluent monolayers of HUVEC in 24-well plates (Costar) were incubated with 100 000 cpm ^{125}I-echistatin in the presence of serial dilutions of RGDPEG−SB−HSA in binding buffer (50 mM Tris−HCl, pH 7.4, 150 mM NaCl, 1 mM $CaCl_2$, 1 mM $MgCl_2$, 1 mM $MnCl_2$, and 1% BSA) at 4 °C for 4 h (*10*). Subsequently, the supernatant was harvested, and cells were washed three times with binding buffer and lysed with 1 M NaOH. Radioactivity was counted in a Packard RIASTAR multiwell gamma counter (GMI, Minnesota). Data were analyzed by nonlinear regression using the GraphPad Prism program (GraphPad Software).

To determine the specificity of RGDPEG−SB−HSA binding and its uptake by target cells, HUVEC were incubated with ^{89}Zr-radiolabeled RGDPEG−SB−HSA. For radiolabeling, 3.73 nmol RGDPEG−SB−HSA was mixed with 18.6 nmol of the chelator TFP−*N*-succinyldesferal−Fe(III) (desferal) (*22*) in 0.1 M $NaHCO_3$, pH 8.5. After an incubation period of 30 min, the reaction mixture was purified on a Hitrap desalting column (GE Healthcare). The conjugation of desferal to the product was confirmed by measurement of its UV absorbance at 430 nm. Fe(III) was replaced with radioactive ^{89}Zr (supplied by Cyclotron BV, Amsterdam) as described (*22*), but the incorporation of zirconium was performed at pH 6.8 and the product was purified using a centricon column (Millipore, Billerica, MA). Radiochemical purity was 96% as determined by trichloroacetic acid precipitation, and specific activity was 740 000 cpm/μg. Specificity of binding was studied by incubating confluent HUVEC layers (24 well plates) with 70 000 cpm ^{89}Zr−RGDPEG−SB−HSA in the presence of an excess of different competitors at 4 °C for 4 h, while uptake was studied by incubating the cells with 70 000 cpm ^{89}Zr−RGDPEG−SB−HSA at 37 °C for 4 h and 8 h. Supernatant and cell-associated radioactivity was harvested as described above, and radioactivity was counted on a 1282 COMPUGAMMA CS (Perkin-Elmer, Boston, MA).

Effect of RGDPEG−SB−HSA on Cell Viability. Platinum-related toxicity of RGDPEG−SB−HSA and ULS-containing intermediate products was evaluated by incubating HUVEC cells for 3 days with EC medium spiked with RGDPEG−SB−HSA (100 μg/mL), SB−ULS (100 μM), ULS (100 μM), or cisplatin (100 μM). The effect on cell proliferation and viability was detected by MTS assay (Promega) according to the manufacturer's protocol.

Effect of RGDPEG−SB−HSA on Inflammatory Events. Effect of targeted SB202190 on transcription and translation of inflammatory genes and proteins was evaluated using quantitative real time PCR (rtPCR) and enzyme-linked immunosorbent assay (ELISA) as described (*23*). In short, confluent monolayers of HUVEC in 12-well plates were incubated with EC medium spiked with RGDPEG−SB−HSA conjugate, RAD-containing control conjugate, free drug, RGDPEG−HSA without drug or an equivalent volume of PBS. After 24 h, the cells were activated by the addition of 5 ng TNFα. After an additional 24 h, medium was harvested, and cells were lysed for RNA isolation (Absolutely RNA Microprep Kit, Stratagene, CA). The amount of isolated RNA was quantified by NanoDrop according to the manufacturer's protocol. Equal amounts of RNA were translated to cDNA by SuperScript III First-Strand Synthesis System (Invitrogen). cDNA was diluted to 10 ng/μL concentration after RT reaction. Exons overlapping primers and Minor Groove Binder (MGB) probes used for RT-PCR were purchased as Assay-on-Demand from Applied Biosystems (Niewekerk a/d IJssel, The Netherlands). Expression levels of human IL-8, E-selectin, and GAPDH were evaluated by RT-PCR on an ABI Prism 7900HT sequence detection system (Applied Biosystems).

Harvested HUVEC supernatants were analyzed for IL-8 production by ELISA using a MoAb.anti-IL-8 (R&D Systems, Minneapolis, MN). The signal was amplified by a biotinylated secondary antibody (polyclonal swine anti-human IL-8; R&D) followed by streptavidin-E+ (CLB, Amsterdam, The Netherlands). Color development was performed using tetramethylbenzidine (Roth, Karlsruhe, Germany) as substrate for the peroxidase.

Statistical Analysis. Statistical analysis was performed using Student's two-tailed *t*-test, assuming equal variances. Difference were considered to be significant when $p < 0.05$ unless otherwise stated.

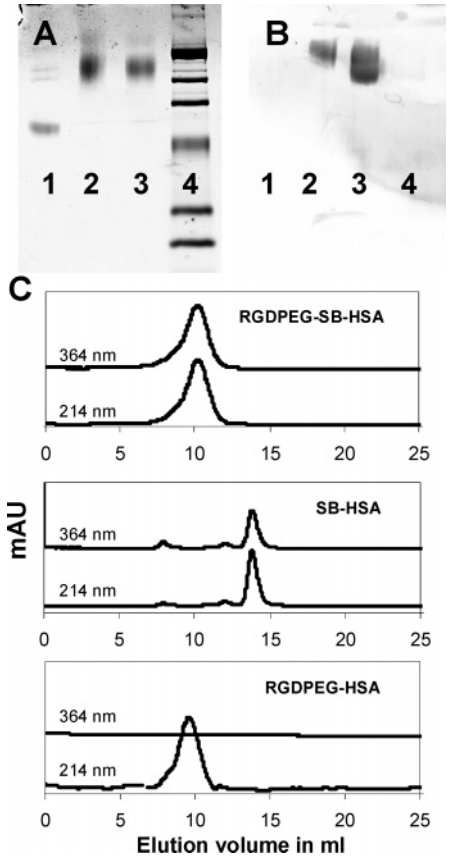

Figure 3. Characterization of RGDPEG−SB−HSA demonstrated successful introduction of SB202190, PEG, and RGD peptide. SDS-PAGE stained for protein with CBB (A) and Western blot with anti RGD antibody (B) of the same gel give proof of RGD-conjugation. The gel shows SB−HSA (1), RGDPEG−SB−HSA (2), RGDPEG−HSA (3), and molecular size marker (4). Size exclusion chromatography (C) demonstrated an increase in size of RGDPEG−SB−HSA compared to SB−HSA detected at 214 nm (bottom line of each graph) due to introduced PEG. SB−ULS absorbed also at 364 nm (upper line of each graph), which is indicative of conjugated SB202190. This peak was detected for RGDPEG−SB−HSA and SB−HSA but not for RGD-PEG−HSA.

RESULTS

Preparation and Characterization of RGDPEG−SB−HSA. We applied a novel type of drug linker to couple SB202190 to our albumin carrier (Figure 2). The ULS linker provided a rapid and straightforward alternative to conventional linkers for conjugation of SB202190. The synthesis of SB−ULS−HSA proceeded at an overall yield of 80% over the combined synthesis steps. In contrast, we also studied the conjugation of SB202190 via ester or carbamate linkages at the hydroxyl group of the drug, which eventually led to products at low yield and undesired fast drug release rates in serum (Prakash et al., submitted).

The first synthesis step between SB202190 and the linker yielded the desired 1:1 SB−ULS species as confirmed by mass spectrometry analysis. ^{1}H NMR studies indicated that binding of SB202190 took place via coordination of the N-donor of the pyridine ring, because only the protons of the pyridyl ring were shifted with the more prominent shift for the protons closest to the nitrogen (8.41 ppm to 8.52 ppm). Additionally, peak splitting was observed for these protons typical for an extra paramagnetic group like platinum. Conjugation of SB−ULS to HSA was confirmed by several techniques. First, the absorbance of SB−ULS at 364 nm was detectable in the SB−HSA product peak, while unmodified albumin had no UV absorption at this wavelength. Monitoring of the 364 nm absorbance also confirmed that SB−ULS remained attached to the carrier during subsequent PEGylation and purification procedures (Figure 3). Second, the drug load of SB−HSA was determined by release of the drug and subsequent HPLC detection (Table 1), and the number of ULS groups attached to the protein was determined by ICP-AES Pt analysis. Both analyses yielded similar numbers of conjugated SB/HSA and ULS/HSA, illustrating that SB202190 was bound to HSA via ULS. Free SB or SB−ULS levels in the conjugate were below the detection limit of the HPLC method (>0.3%).

The SB−HSA product was modified with RGD peptides via a 3.5 kDa PEG linker. Successful PEGylation and purity of the product was shown by size exclusion chromatography (SEC, Figure 3). SEC also revealed the absence of aggregates. Final proof of binding of the RGD peptide to the distal end of the PEG-linker was given by SDS-PAGE and Western blot with an anti-RGD antibody (Figure 3). The molecular weight (MW) of the products was determined by MALDI-TOF analysis, and differences in MW were used to calculate the number of RGDPEG bound per albumin (Table 1). On average, SB−ULS−HSA was modified with 6.3 RGDPEG/HSA, while 7.1 RGD-PEG/HSA were bound to parental HSA.

SB202190 is Released via Competition with Sulfur Donors. We studied the stability and release properties of the novel SB−ULS−HSA conjugate in different conditions. All incubations were performed at 37 °C for 24 h (Figure 4). Only minimal drug release was observed in buffers or culture medium containing 20% serum, indicating the high stability of the SB202190−ULS linkage. However, addition of thiols like GSH and DTT accelerated the release of the drug. Complete release of the drug could be effected by incubating the conjugate at 80° C with a large excess of the thiocyanate (data not shown). Since thiols are preferred ligands for platinum, competitive displacement seems a likely release mechanism. These results are in good agreement with prior studies in our group with other drug−ULS−albumin (*24*). Changing the pH from 7.4 (cytosolic) to pH 5.0 (lysosomal) gave a reduction in drug release by DTT, while GSH-induced release was not affected.

RGDPEG−SB−HSA Binds via $\alpha_v\beta_3$-Integrin to Target Cells and Is Internalized. Binding constants of RGDPEG−SB−HSA for target cells have been evaluated in competition experiments with the known $\alpha_v\beta_3$-integrin ligand ^{125}I-echistatin as shown in Figure 5A. The RGDPEG−SB−HSA conjugate demonstrated a higher affinity for $\alpha_v\beta_3$-integrin (IC_{50} = 71.4 nM; Table 2) compared to the single peptide (IC_{50} = 383 nM), but a lower affinity than RGDPEG−HSA (IC_{50} = 11.7 nM), which had been equipped with a higher amount of RGD groups.

Table 1. Characterization of Drug Targeting Conjugates (n.a., not applicable; n.d. not determined; −, negative; +, positive)

	number of SB bound per HSA[a]	number of ULS bound per HSA[a]	number of RGDPEG bound per HSA[b]	MW in kDa[b]	Western blot for RGD[b]
SB−HSA	9.1	7.8	n.a.	69.2	−
RGDPEG−SB−HSA	9.6	8.0	6.3	95.2	+
RADPEG−SB−HSA	7.6	6.1	n.d.	n.d	n.a.
RGDPEG−HSA	n.a.	n.a.	7.1	96.1	+

[a] average of duplicate analysis. [b] single analysis.

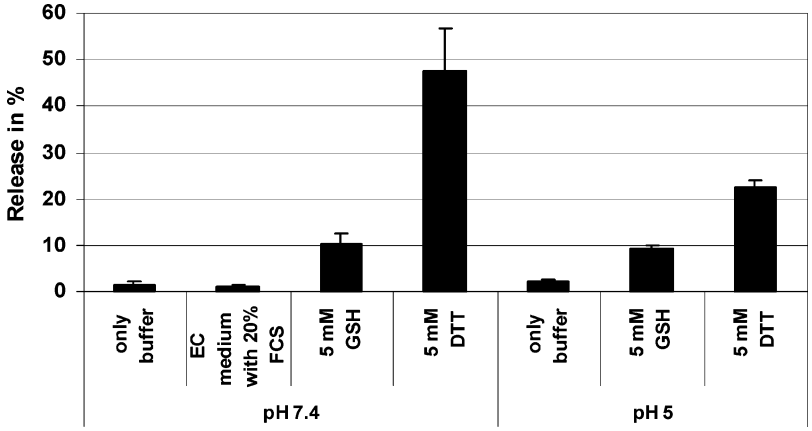

Figure 4. Release of SB202190. SB−ULS−HSA was incubated for 24 h at 37 °C with 5 mM GSH or DTT at pH 5 in acetic acid buffer or at pH 7.4 in PBS and in endothelial cell medium with 20% FCS. Released drug was determined by HPLC.

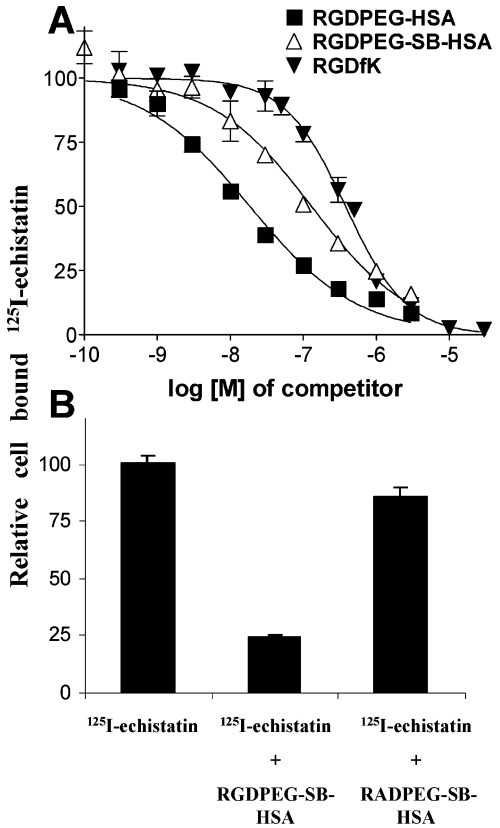

Figure 5. Binding properties of RGDPEG−SB−HSA. (A) shows competitive displacement of ^{125}I-echistatin with RGDPEG−HSA (squares), RGDPEG−SB−HSA (open triangles), and RGDfK (closed triangles). (B) demonstrates displacement of ^{125}I-echistatin by RGD-PEG−SB−HSA but not by control conjugate RADPEG−SB−HSA, both at 1 μM.

Table 2. IC_{50} of Binding to $\alpha_v\beta_3$-Integrin and the Fold Increase in Affinity Compared to the Single Peptide

	IC_{50} in nM	fold increase in affinity
RADfK	>10 000	−
RADPEG−SB−HSA	>3000	−
RGDfK	383	1
RGDPEG−SB−HSA	71.4	5.4
RGDPEG−HSA	11.7	33

RADPEG−SB−HSA could not displace ^{125}I-echistatin at any of the concentrations tested (Figure 5B).

We also studied binding and uptake of ^{89}Zr−RGDPEG−SB−HSA by endothelial cells. ^{89}Zr, captured by the chelator desferal, is highly stable, and its hydrophilicity will entrap it inside cells after degradation of the carrier (*25*, *26*). Since this will prevent redistribution of the radiolabel, Zr−desferal is an ideal label for uptake studies. We attached an average of 1.7 desferal groups/HSA, which were subsequently loaded with ^{89}Zr. Such a relatively minor modification will not affect the binding of RGDPEG−SB−HSA to target cells, as was also demonstrated by comparing the binding of ^{125}I and ^{89}Zr-labeled RGDPEG−SB−HSA (data not shown). Furthermore, the extended nature of the RGDPEG ligand will prevent steric interactions between radiotracer and RGD groups.

^{89}Zr−RGDPEG−SB−HSA was incubated at 4 °C and 37 °C with HUVEC. ^{89}Zr−RGDPEG−SB−HSA binding to $\alpha_v\beta_3$-expression HUVEC could only be blocked by excess of RGD peptide but not by excess of SB−HSA (Figure 6A). This proved that binding was solely mediated by the introduced RGD peptide. Cell-associated activity was increased when incubation were carried out at 37 °C and could be further increased with prolonged incubation times (Figure 6B). This indicated active uptake of RGDPEG−SB−HSA into endothelial cells.

RGDPEG−SB−HSA Is Not Toxic to Endothelial Cells. RGDPEG−SB−HSA, SB−ULS, and free ULS tested at 100 μM did not influence the proliferation and viability of HUVEC (Figure 7). In the same concentration, cisplatin eradicated all cells, suggesting that both monofunctional ULS derivatives as well as bifunctional ULS mononitratemonochloride are not toxic, whereas cisplatin (bifunctional) is.

Effect of RGDPEG−SB−HSA on Activated HUVEC. The anti-inflammatory effects of the conjugate were investigated in TNF-activated HUVEC. TNFα induced a 20-fold upregulation in gene expression of hIL-8 and 200-fold upregulation of hE-selectin (Figure 8). Free SB202190 inhibited this upregulation up to 50%, which is in agreement with previous studies (*23*). RGDPEG−SB−HSA was tested at 21 μg/mL and 70 μg/mL, which corresponds to a drug concentration of 3 μM and 10 μM, respectively. Significant down-regulation of the studied genes was observed in all conditions, except for hE-selectin when cells were incubated with a low concentration of RGDPEG−SB−HSA. Expression of both genes was reduced for approximately 30% compared to the TNF-activated control cells ($p < 0.01$). RGDPEG−HSA, i.e., carrier without drug, and nontargeted conjugate RADPEG−SB−HSA demonstrated no inhibitory effect. RGDPEG−HSA showed even a slight upregulation of the tested genes, especially when given in the higher dose.

Similar inhibitory effects of the delivered drug were observed when IL-8 secretion in the culture medium was analyzed (Figure 9). RGDPEG−SB−HSA at both concentrations reduced the IL-8 secretion by 18% and 34% as compared to untreated cells

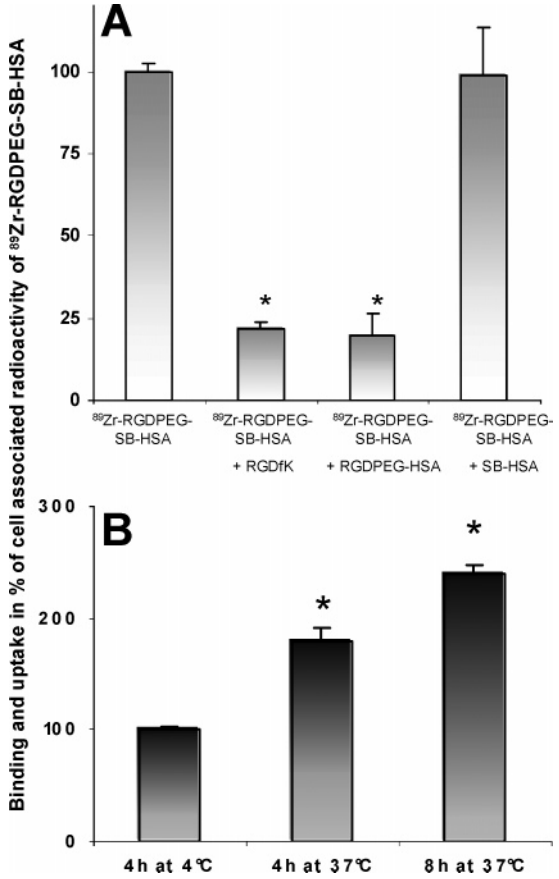

Figure 6. RGDPEG−SB−HSA binds via the introduced RGD moiety to target cells and is internalized. (A) ^{89}Zr−RGDPEG−SB−HSA was incubated with a confluent HUVEC monolayer. The addition of high excess of different competitors (RGDfK, 20 μM; RGDPEG−HSA, 1 μM; SB−HSA, 1 μM) demonstrated that RGDPEG−SB−HSA only bound via the RGD-peptide. (B) HUVEC were incubated with ^{89}Zr−RGDPEG−SB−HSA at 4 and 37 °C for 4 and 8 h to determine uptake of the drug-targeting conjugate. *$p < 0.01$ compared to no competitor in (A) and to 4 °C in (B).

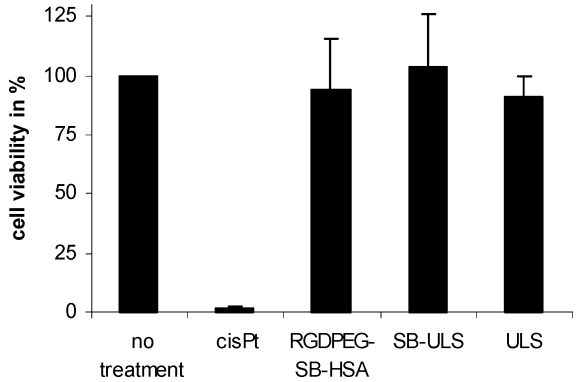

Figure 7. RGDPEG−SB−HSA and ULS containing conjugates displayed no toxicity for endothelial cells. RGDPEG−SB−HSA (100μg/mL), SB−ULS, ULS, or cisplatin (all at 100 μM) were added to EC medium and incubated for 3 days. Cell viability was assessed in comparison to nontreated control cells (=100% viability) using MTS assay.

($p < 0.01$). Control conjugates did not decrease levels of IL-8 in the medium.

DISCUSSION

In the present study, we developed an endothelial-directed conjugate for cell-specific intracellular delivery of SB202190, a potent p38MAPK inhibitor (Figure 1). We applied a novel

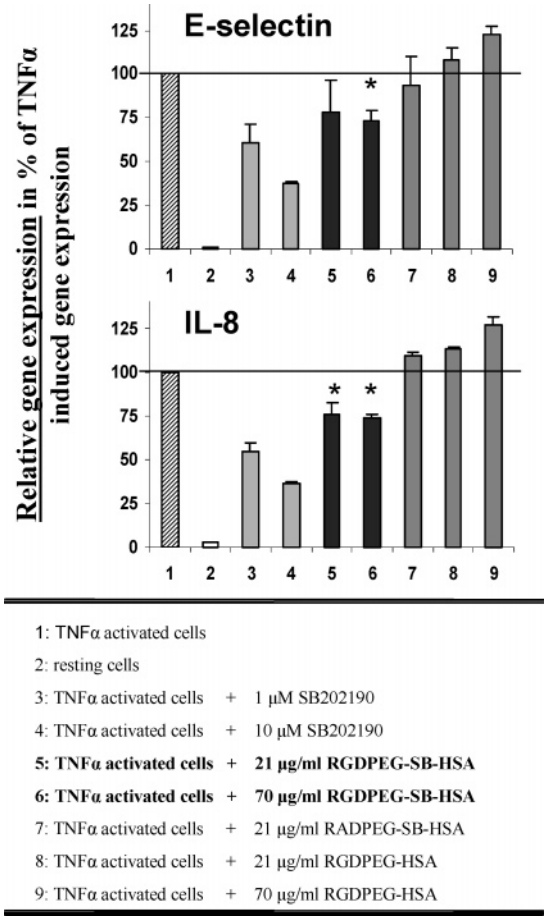

Figure 8. RGDPEG−SB−HSA delivered active SB202190 into target cells. HUVEC were preincubated with drug, drug-targeting conjugate, and control conjugates for and 24 h, after which TNFα was added. RNA was harvested after an additional 24 h of incubation. Gene expression levels of hE-selectin and hIL-8 as determined by qRT-PCR are shown. Light gray bars represent free drug, black bars represent drug-targeting conjugate, and dark gray bars represent different control conjugates. 21 μg/mL of RGDPEG−SB−HSA equals 3 μM SB202190 and 70 μg/mL equals 10 μM drug. $p < 0.01$ compared to respective control conjugates and to TNFα-treated control.

type of platinum linker for coupling of SB202190 to albumin, which provided a straightforward and robust coupling method (Figure 2). The conjugation of ULS with SB202190 took place by formation of a coordinative bond between the nitrogen of the pyridine and the Pt atom. Since aromatic nitrogens are present in many drug structures, our approach is applicable to many other drugs besides SB202190. We have recently reported on a similar linkage approach for the delivery of pentoxifyllin to hepatic stellate cells (*24*), and several other conjugates are under investigation.

We assume that the drug−ULS adduct binds to HSA by coordination to sulfur-containing residues, mostly methionine, but also with histidine residues as demonstrated earlier for other Pt(II) compounds (*27*, *28*). Our hypothesis that SB−ULS preferably binds to sulfur groups in the carrier is supported by the finding that pentoxifyllin−ULS/albumin conjugation ratios increased when HSA was first modified with a thiocarbonyl-containing targeting ligand (*24*). Similarly, elevated drug−ULS/carrier ratios were found when the kidney-selective carrier lysozyme was modified with extra methionine groups (J. Prakash et al., submitted). HSA contains only six methionine residues, which are not exposed at the protein surface. The hydrophobic character of SB−ULS will allow its binding to methionines in the core of HSA. As the number of SB−ULS per HSA exceeded

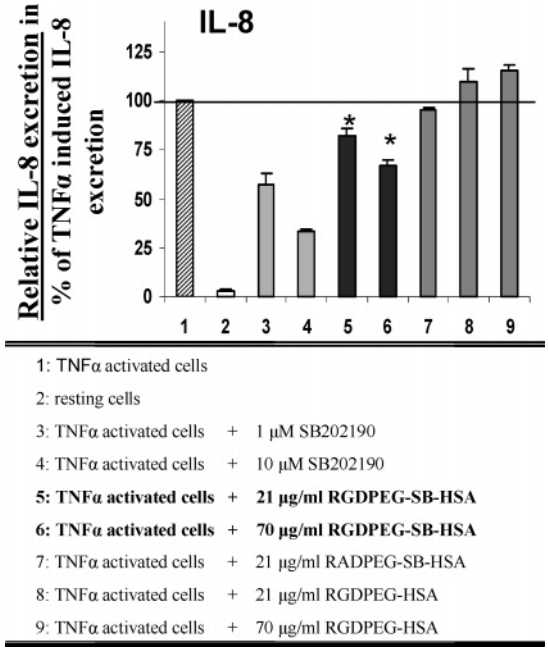

Figure 9. RGDPEG−SB−HSA treatment reduced the excretion of IL-8. HUVEC were preincubated with drug, drug-targeting conjugate, and control conjugates, and 24 h later, TNF was added. Medium was harvested after an additional 24 h of incubation. Relative levels of hIL-8 as determined by ELISA are depicted in the graph. Light gray bars represent free drug, black bars represent drug-targeting conjugate, and dark gray bars represent different control conjugates. 21 μg/mL of RGDPEG−SB−HSA equals 3 μM SB202190 and 70 μg/mL equals 10 μM SB202190. $p < 0.01$ compared to respective control conjugates and to TNFα-treated control.

the number of available methionines, it seems likely that SB−ULS is also bound to histidine or cysteine residues.

We assume that SB202190 needs to be released from the linker to exert therapeutic effects, since the pyridyl ring of SB202190 to which ULS is bound is also interacting with the ATP pocket of the p38 MAP kinase. Release of SB202190 was triggered by competition with sulfur ligands like glutathione at intracellular concentration. We have found the same release mechanism for other drug−ULS conjugates (Prakash et al., submitted) (*24*).

Conjugation of PEG and RGD peptide to SB−HSA resulted in a macromolecular conjugate that was characterized by several techniques. MALDI-TOF analysis illustrated that further modification of SB−HSA is not hampered by already bound SB202190−ULS. This was expected, given that ULS binds best to methionine residues, but also to cysteine and histidine residues, while the PEG linker reacted with amino groups of, e.g., lysine residues. The kind of RGD peptide (c(RGDfK)) used in this study binds specifically and with a high affinity to $\alpha_v\beta_3$-integrin due to the special constrained conformation. We now show that these properties are transferred to SB−HSA upon conjugation of RGD peptides. The 5.4-fold improvement in binding affinity as compared to the single peptide indicates multivalent binding of the conjugate. This is in line with earlier observations of Kok et al. (*9*) and is also relevant for receptor-mediated uptake of the conjugate, since multivalency is known to facilitate internalization and routing to lysosomes (*11*, *29*).

Platinum is an intrinsic component of ULS, and this prompted us to evaluate potential toxicity of the drug-targeting conjugate, and of ULS in particular. It is generally accepted that cisplatin toxicity involves cross-linking of DNA (*30*). The availability of a reactive ligand site at the platinum atom is essential for the toxicity of platinum(II) compounds. However, the platinum atom in RGDPEG−SB−HSA is fully coordinated, which prevents its binding with endogenous compounds. ULS can therefore only react with DNA after release of the drug or carrier. In view of the slow drug release from the construct, we expect only a slow formation of reactive platinum species in the target cells that will readily detoxified, as described for cisplatin and other platinum compounds (*31*, *32*). The absence of toxicity on HUVEC viability of ULS-containing compounds was clearly demonstrated even at high concentrations (Figure 7). Likely, glutathione adducts will be the major metabolite. We concluded that drug−ULS conjugates have no apparent toxicity despite their similarity to cisplatin. The same conclusion has been drawn for other ULS-containing drug-targeting conjugates that have been developed in our lab for the targeting to hepatic stellate cells (*24*) or kidney tubular cells (Prakash et al., submitted).

RGDPEG−SB−HSA partially inhibited the TNFα-induced activation of HUVEC, both at gene expression levels and when considering the secretion of proinflammatory cytokines (Figures 8 and 9). Since premature drug release in endothelial cell medium can be excluded on the basis of the drug release studies, we concluded that SB202190 was released after internalization of RGDPEG−SB−HSA. Although RGDPEG−SB−HSA demonstrated the anticipated effects, the observed inhibitions were lower than those of free SB202190. Several considerations may explain these differences. First, the different uptake mechanisms of conjugate and free drug will affect intracellular drug levels. The passive diffusion of a small molecule drug will be faster than the active uptake process and subsequent lysosomal degradation of a high molecular weight drug-targeting conjugate. Typically, inhibiting drugs are preincubated with the cells for about 1 h. Since such a short period would allow only limited uptake of the conjugate, we have preincubated the cells for 24 h with the compounds. Apparently, this had not resulted in extensive accumulation of active drug in the cells. Another explanation may be that intracellularly released SB202190 diffused out of the target cells. Such a redistribution of the compound by diffusion or active transport might limit the applicability of such conjugates in vivo. It therefore seems interesting to study the intracellular drug levels of free and conjugate-bound drug. This, however, proved to be impossible with the available HPLC techniques, as these have a relatively low sensitivity. Alternatively, one might prevent redistribution by delivering charged or hydrophilic drug molecules.

When considering the in vivo applicability of our approach, several studies support our strategy. The feasibility of RGD-mediated targeting for chronic inflammatory disorders has been demonstrated by RGD-peptide imaging agents that specifically accumulate in chronically inflamed tissue but not in acutely inflamed tissue (*33*, *34*). Furthermore, Gerlag et al. have treated mice suffering from collagen-induced arthritis with an RGD-targeted proapoptotic peptide (*35*). Their approach induced apoptosis of synovial blood vessels and significantly decreased clinical arthritis. We, however, aimed for the development of a therapeutic agent that can block inflammatory signaling pathways without compromising the viability of the vasculature. We furthermore expect improved pharmacokinetics of our macromolecular product as compared to smaller peptides or free SB202190. Free SB202190 is rapidly cleared from the circulation with a $t_{1/2}\alpha$ of 4.3 min in rats and has no affinity for inflamed tissue (*36*). In contrast, RGDPEG−SB−HSA can accumulate in inflamed endothelium in analogy to the RGD-peptide-based imaging agents. The long PEG linker will shield the modified albumin to prevent unspecific uptake and can increase the circulation time (*37*). Passive retention of the PEGylated drug carrier might also occur due to enhanced permeability of endothelium in inflamed tissues (*14*). In principle, RGDPEG−SB−HSA will be administered intravenously rather than by local injection in the joints. Since the

endothelium is in direct contact with the systemic circulation, these target cells can be reached from within the circulation. Thus, painful injections into inflamed joints would not be necessary.

In conclusion, we have prepared a novel drug-targeting conjugate in which we linked the drug via platinum coordination chemistry to the carrier. This RGDPEG−SB−HSA bound with high affinity and specificity to $\alpha_v\beta_3$-integrin and was subsequently internalized. The delivered drug was furthermore capable of interfering in inflammatory signaling cascades. These results show the potential of MAPkinase inhibitor delivery as a new strategy to counteract chronic inflammatory disorders.

ACKNOWLEDGMENT

J. H. Pol from the Department of Nuclear Medicine is kindly acknowledged for radiolabeling of echistatin, H. E. Moorlag from the Endothelial Cell Facility UMCG for skillful isolation and culturing of HUVEC, B. Doornbos-van der Meer for assistance with ELISA, and J. Ijmker for platinum detection using ICP-AES. We also acknowledge Prof. G. A. M. S. van Dongen and Ir. L. R. Perk of the VUmc for providing the desferal labeling technology. Our colleagues from KREATECH are acknowledged for critical review of the manuscript. This work was made possible by grants from Marie Curie (HPMI-CT-2002-00218), SenterNovem (TSGE1083), and Hungarian Scientific Research Fund OTKA (T-049478).

LITERATURE CITED

(1) Schett, G., Tohidast-Akrad, M., Smolen, J. S., Schmid, B. J., Steiner, C. W., Bitzan, P., Zenz, P., Redlich, K., Xu, Q., and Steiner, G. (2000) Activation, differential localization, and regulation of the stress-activated protein kinases, extracellular signal-regulated kinase, c-JUN N-terminal kinase, and p38 mitogen-activated protein kinase, in synovial tissue and cells in rheumatoid arthritis. *Arthritis Rheum. 43*, 2501−2512.

(2) Griffioen, A. W., and Molema, G. (2000) Angiogenesis: potentials for pharmacologic intervention in the treatment of cancer, cardiovascular diseases, and chronic inflammation. *Pharmacol. Rev. 52*, 237−268.

(3) Szekanecz, Z., and Koch, A. E. (2004) Vascular endothelium and immune responses: implications for inflammation and angiogenesis. *Rheum. Dis. Clin. North Am. 30*, 97−114.

(4) Kuldo, J. M., Ogawara, K. I., Werner, N., Asgeirsdottir, S. A., Kamps, J. A., Kok, R. J., and Molema, G. (2005) Molecular pathways of endothelial cell activation for (targeted) pharmacological intervention of chronic inflammatory diseases. *Curr. Vasc. Pharmacol. 3*, 11−39.

(5) Karin, M. (2005) Inflammation-activated protein kinases as targets for drug development. *Proc. Am. Thorac. Soc. 2*, 386−390.

(6) Schieven, G. L. (2005) The biology of p38 kinase: a central role in inflammation. *Curr. Top. Med. Chem. 5*, 921−928.

(7) Smolen, J. S., and Steiner, G. (2003) Therapeutic strategies for rheumatoid arthritis. *Nat. Rev. Drug Discovery 2*, 473−488.

(8) Kumar, S., Boehm, J., and Lee, J. C. (2003) p38 MAP kinases: key signalling molecules as therapeutic targets for inflammatory diseases. *Nat. Rev. Drug Discovery 2*, 717−726.

(9) Kok, R. J., Schraa, A. J., Bos, E. J., Moorlag, H. E., Asgeirsdottir, S. A., Everts, M., Meijer, D. K., and Molema, G. (2002) Preparation and functional evaluation of RGD-modified proteins as alpha(v) beta-(3) integrin directed therapeutics. *Bioconjugate Chem. 13*, 128−135.

(10) Schraa, A. J., Kok, R. J., Berendsen, A. D., Moorlag, H. E., Bos, E. J., Meijer, D. K., de Leij, L. F., and Molema, G. (2002) Endothelial cells internalize and degrade RGD-modified proteins developed for tumor vasculature targeting. *J. Controlled Release 83*, 241−251.

(11) Schraa, A. J., Kok, R. J., Moorlag, H. E., Bos, E. J., Proost, J. H., Meijer, D. K., de Leij, L. F., and Molema, G. (2002) Targeting of RGD-modified proteins to tumor vasculature: a pharmacokinetic and cellular distribution study. *Int. J. Cancer 102*, 469−475.

(12) Beljaars, L., Poelstra, K., Molema, G., and Meijer, D. K. (1998) Targeting of sugar- and charge-modified albumins to fibrotic rat livers: the accessibility of hepatic cells after chronic bile duct ligation. *J. Hepatol. 29*, 579−588.

(13) van Gijlswijk, R. P., Talman, E. G., Janssen, P. J., Snoeijers, S. S., Killian, J., Tanke, H. J., and Heetebrij, R. J. (2001) Universal Linkage System: versatile nucleic acid labeling technique. *Expert Rev. Mol. Diagn. 1*, 81−91.

(14) Maeda, H., Fang, J., Inutsuka, T., and Kitamoto, Y. (2003) Vascular permeability enhancement in solid tumor: various factors, mechanisms involved and its implications. *Int. Immunopharmacol. 3*, 319−328.

(15) Pablos, J. L., Santiago, B., Galindo, M., Torres, C., Brehmer, M. T., Blanco, F. J., and Garcia-Lazaro, F. J. (2003) Synoviocyte-derived CXCL12 is displayed on endothelium and induces angiogenesis in rheumatoid arthritis. *J. Immunol. 170*, 2147−2152.

(16) Creamer, D., Allen, M., Sousa, A., Poston, R., and Barker, J. (1995) Altered vascular endothelium integrin expression in psoriasis. *Am. J. Pathol. 147*, 1661−1667.

(17) Eliceiri, B. P., and Cheresh, D. A. (1999) The role of alphav integrins during angiogenesis: insights into potential mechanisms of action and clinical development. *J. Clin. Invest. 103*, 1227−1230.

(18) Schraa, A. J., Everts, M., Kok, R. J., Asgeirsdottir, S. A., Meijer, D. K., de Leij, L. F., and Molema, G. (2002) Development of vasculature targeting strategies for the treatment of cancer and chronic inflammatory diseases. *Biotechnol. Annu. Rev. 8*, 133−165.

(19) Mulder, A. B., Blom, N. R., Smit, J. W., Ruiters, M. H., van der, M. J., Halie, M. R., and Bom, V. J. (1995) Basal tissue factor expression in endothelial cell cultures is caused by contaminating smooth muscle cells. Reduction by using chymotrypsin instead of collagenase. *Thromb. Res. 80*, 399−411.

(20) Kumar, C. C., Nie, H., Rogers, C. P., Malkowski, M., Maxwell, E., Catino, J. J., and Armstrong, L. (1997) Biochemical characterization of the binding of echistatin to integrin alphavbeta3 receptor, *J. Pharmacol. Exp. Ther. 283*, 843−853.

(21) Hunter, W. M., and Greenwood, F. C. (1962) Preparation of iodine-131 labelled human growth hormone of high specific activity. *Nature (London) 194*, 495−496.

(22) Verel, I., Visser, G. W., Boellaard, R., Stigter-van, W. M., Snow, G. B., and van Dongen, G. A. (2003) 89Zr immuno-PET: comprehensive procedures for the production of 89Zr-labeled monoclonal antibodies. *J. Nucl. Med. 44*, 1271−1281.

(23) Kuldo, J. M., Westra, J., Asgeirsdottir, S. A., Kok, R. J., Oosterhuis, K., Rots, M. G., Schouten, J. P., Limburg, P. C., and Molema, G. (2005) Differential effects of NF-{kappa}B and p38 MAPK inhibitors and combinations thereof on TNF-{alpha}- and IL-1{beta}-induced proinflammatory status of endothelial cells in vitro. *Am. J. Physiol. Cell Physiol. 289*, C1229−C1239.

(24) Gonzalo, T., Talman, E. G., van, d., V, Temming, K., Greupink, R., Beljaars, L., Reker-Smit, C., Meijer, D. K., Molema, G., Poelstra, K., and Kok, R. J. (2006) Selective targeting of pentoxifylline to hepatic stellate cells using a novel platinum-based linker technology. *J. Controlled Release 111*, 193−203.

(25) Verel, I., Visser, G. W., Boerman, O. C., van Eerd, J. E., Finn, R., Boellaard, R., Vosjan, M. J., Stigter-van Walsum, M., Snow, G. B., and van Dongen, G. A. (2003) Long-lived positron emitters zirconium-89 and iodine-124 for scouting of therapeutic radioimmunoconjugates with PET. *Cancer Biother. Radiopharm. 18*, 655−661.

(26) Perk, L. R., Visser, G. W., Vosjan, M. J., Stigter-van, W. M., Tijink, B. M., Leemans, C. R., and van Dongen, G. A. (2005) (89)-Zr as a PET surrogate radioisotope for scouting biodistribution of the therapeutic radiometals (90)Y and (177)Lu in tumor-bearing nude mice after coupling to the internalizing antibody cetuximab. *J. Nucl. Med. 46*, 1898−1906.

(27) Cox, M. C., Barnham, K. J., Frenkiel, T. A., Hoeschele, J. D., Mason, A. B., He, Q. Y., Woodworth, R. C., and Sadler, P. J. (1999) Identification of platination sites on human serum transferrin using (13)C and (15)N NMR spectroscopy. *J. Biol. Inorg. Chem. 4*, 621−631.

(28) Trynda-Lemiesz, L., Kozlowski, H., and Keppler, B. K. (1999) Effect of cis-, trans-diamminedichloroplatinum(II) and DBP on human serum albumin. *J. Inorg. Biochem. 77*, 141−146.

(29) Boturyn, D., Coll, J. L., Garanger, E., Favrot, M. C., and Dumy, P. (2004) Template assembled cyclopeptides as multimeric system for integrin targeting and endocytosis. *J. Am. Chem. Soc. 126*, 5730−5739.

(30) Fuertes, M. A., Castilla, J., Alonso, C., and Perez, J. M. (2002) Novel concepts in the development of platinum antitumor drugs, *Curr. Med. Chem.: Anti-Cancer Agents 2*, 539−551.

(31) Sadowitz, P. D., Hubbard, B. A., Dabrowiak, J. C., Goodisman, J., Tacka, K. A., Aktas, M. K., Cunningham, M. J., Dubowy, R. L., and Souid, A. K. (2002) Kinetics of cisplatin binding to cellular DNA and modulations by thiol-blocking agents and thiol drugs. *Drug Metab. Dispos. 30*, 183−190.

(32) Volckova, E., Dudones, L. P., and Bose, R. N. (2002) HPLC determination of binding of cisplatin to DNA in the presence of biological thiols: implications of dominant platinum-thiol binding to its anticancer action. *Pharm. Res. 19*, 124−131.

(33) Pichler, B. J., Kneilling, M., Haubner, R., Braumuller, H., Schwaiger, M., Rocken, M., and Weber, W. A. (2005) Imaging of Delayed-Type Hypersensitivity Reaction by PET and 18F-Galacto-RGD. *J. Nucl. Med. 46*, 184−189.

(34) Lewis, M. R. (2005) Radiolabeled RGD Peptides Move Beyond Cancer: PET Imaging of Delayed-Type Hypersensitivity Reaction. *J. Nucl. Med. 46*, 2−4.

(35) Gerlag, D. M., Borges, E., Tak, P. P., Ellerby, H. M., Bredesen, D. E., Pasqualini, R., Ruoslahti, E., and Firestein, G. S. (2001) Suppression of murine collagen-induced arthritis by targeted apoptosis of synovial neovasculature. *Arthritis Res. 3*, 357−361.

(36) Prakash, J., Saluja, V., Visser, J., Moolenaar, F., Meijer, D. K., Poelstra, K., and Kok, R. J. (2005) Bioanalysis and pharmacokinetics of the p38 MAPkinase inhibitor SB202190 in rats. *J. Chromatogr., B 826*, 220−225.

(37) Caliceti, P., and Veronese, F. M. (2003) Pharmacokinetic and biodistribution properties of poly(ethylene glycol)−protein conjugates. *Adv. Drug Delivery Rev. 55*, 1261−1277.

BC0600158